Chinese Chemical Letters 32 (2021) 119–124

Contents lists available at ScienceDirect

Chinese Chemical Letters

journal homepage: www.elsevier.com/locate/cclet

Communication

Metal-organic framework derived NiCoP hollow polyhedrons electrocatalyst for pH-universal hydrogen evolution reaction

Yunrui Wei, Xixi Zhang, Zonghua Wang, Jiangmei Yin, Jinzhao Huang, Gang Zhao*, Xijin Xu*

School of Physics and Technology, University of Jinan, Ji'nan 250022, China

ARTICLE INFO

Article history:
Received 19 July 2020
Received in revised form 30 September 2020
Accepted 29 October 2020
Available online 1 November 2020

Keywords:
Hollow structure
ZIF-67
NiCoP
Hydrogen evolution reaction
pH-Universal range

ABSTRACT

Hollow nanostructures have attracted increasing research interest in hydrogen evolution reaction owing to their unique structural features. Herein, Ni–Co mixed metal phosphide hollow and porous polyhedrons was successfully composited (expressed as NiCoP). Benefiting from the synergistic effects of ZIF-67 by doping Ni elements and the well-defined hollow and porous structure, the as-synthesized NiCoP hollow and porous polyhedrons exhibit better electrochemical properties and mechanical stability for hydrogen evolution reaction over a pH-universal range, with a small Tafel slopes of 72, 101, 176 mV/dec, and a low overpotential of 82, 102, 261 mV at a current density of 10 mA/cm^2 in 0.5 mol/L H_2SO_4, 1 mol/L KOH and 1 mol/L phosphate buffer solution (PBS). This general strategy can also be applied to fabricate other hollow cobalt-based phosphides and MOFs-derived materials for HER.

Fabricate and design of complex nanostructures are extensively discussed based on their structural features and compositional merits. Amongst the myriad nanostructures, hollow nanostructures are of great interest because of their structural merits and have shown potential applications in various fields in recent years [1–3]. In particular, hollow nanostructures with higher surface-to-volume ratios and unique structural features hold great promise as electrode materials for water splitting electrolyzers and hybrid supercapacitors [4]. Most hollow structured MOF derivatives are synthesized through thermal treatments or ion exchange reactions under appropriate conditions.

Metal-organic frameworks (MOF) possessing intriguing structures and abundant coordination centers have been widely investigated as versatile precursors to prepare transition metal materials [5–9]. For examples, Co_3O_4 [10], Fe_2O_3 [11], $NiCo_2O_4$ [12], having novel morphologies, can be obtained by directly annealing MOFs in air. The controlled etching method is generally used to create hollow space by selectively dissolving the inner part of solid MOF precursors [13]. Zeolitic imidazolate frameworks (ZIF), such as ZIF-67 [14–16] and ZIF-8 [17], are a novel class of porous materials with zeolite-like 3D topological structures, abundant carbon and nitrogen ligands, and high metal ion contents and are expected to be good candidates as the precursor template to design various porous nanostructured metal-carbon hybrid materials and the corresponding phosphide derivatives. The metal incorporated porous carbon has high surface area and can be used to fabricate electrodes for proton exchange membrane fuel cell, lithium ion battery, and so on [18,19].

Transition metal phosphides (TMP) have emerged as advanced HER catalysts in pH-universal range due to their excellent conductivity and analogous active sites in hydrogenases with strong ability of attracting protons [20,21]. For example, Feng *et al.* have synthesized porous nickel–cobalt phosphide nanocubes *via* a template-engaged strategy using Prussian blue analogues as precursors [22]. They found that the synergistic effect between the two phases (Ni_2P and CoP) has great contribution to the excellent HER performance, which suggests that metal phosphides with complex compositions may improve the electrocatalytic activity compared to single phase metal phosphides. A hybrid catalyst combining TMP and MOF, if appropriately designed, may not only possesses an optimal ΔGH^* but also takes advantage of MOF's well-defined porous structure, both of which are beneficial to HER performance.

In this work, we demonstrate a facile and economical three-step preparation of Ni–Co mixed metal phosphide hollow polyhedrons. The thermal conversion of the etched MOFs method can be also applied to other metal-doping systems. When used as an HER electrocatalyst, the NiCoP hollow polyhedrons exhibits extraordinary pH-universal Pt-like activity and high stability, with overpotentials of 82, 102 and 261 mV at the current density of

* Corresponding authors.
E-mail addresses: sps_zhaog@ujn.edu.cn (G. Zhao), sps_xuxj@ujn.edu.cn (X. Xu).

https://doi.org/10.1016/j.cclet.2020.10.046
1001-8417/

10 mA/cm^2 in 0.5 mol/L H_2SO_4, 1 mol/L KOH and 1 mol/L phosphate buffer solution (PBS, pH 7.0), respectively. This work could open a door to the design and modification of high performance electrocatalysts based on MOFs.

ZIF67 was prepared according to the literature [23]. Typically, two solutions were first prepared by dissolving 5 mmol of $Co(NO_3)_2{\cdot}6H_2O$ and 20 mmol of 2-methylimidazole in 50 mL of methanol. Then, the solution of 2-methylimidazole was quickly poured into the solution of $Co(NO_3)_2$ and the resultant mixed purple solution was aged for 24 h at room temperature. The purple precipitate was obtained by centrifugation and dried in vacuum at 60 °C for 12 h.

Next, what is very important in the experiment is the synthesis of ZIF-67@Ni-Co LDH, $Co_3O_4/NiCo_2O_4$ Yolk-shelled Polyhedrons and Co_3O_4 polyhedrons. Firstly, 0.152 g $Ni(NO_3)_2{\cdot}6H_2O$ was dissolved in 50 mL ethanol. Then 0.076 g ZIF-67 was dispersed in 10 mL ethanol, the dispersion was quickly poured into the former solution. After stirring for 60 min, the mixed solution was allowed standing for 1 h at room temperature. An aquamarine blue precipitate was formed and collected by centrifugation, following by washing with ethanol and dried in vacuum overnight. Similarly, the morphology of ZIF-67@Ni-Co LDH particles can be easily modulated by varying the mass ratio of ZIF-67 to $Ni(NO_3)_2{\cdot}6H_2O$. Finally, the $Co_3O_4/NiCo_2O_4$ yolk-shelled polyhedrons were obtained by annealing the as-obtained structure of yolk-shelled polyhedron in air at 300 °C for 2 h with a ramp rate of 1 °C/min.

The Co_3O_4 polyhedrons were obtained according to the reported method. Firstly, 100 mg ZIF-67 was put in a tube furnace and heated with a rate of 1 °C/min and maintained at 300 °C for 2 h under Ar gas flow.

The $Co_3O_4/NiCo_2O_4$ yolk-shelled polyhedrons (100 mg) were put in a tube furnace, and 500 mg of $NaH_2PO_2{\cdot}H_2O$ was placed at the upstream side. Under Ar gas, the temperature of the furnace was heated to 300 °C at a rate of 2 °C/min and maintained for 1 h. After the system was cooled to ambient temperature under Ar, the final products were denoted as NiCoP hollow polyhedrons.

CoP polyhedrons were synthesized with the same method except the precursor was Co_3O_4 polyhedrons. The morphology and structure of NiCoP hollow polyhedrons and its precursors were characterized by field-emission scanning electron microscopy (FESEM, JSM-6700 F, Japan) with energy dispersive X-ray spectroscopy (EDS), and transmission electron microscopy (TEM; JEOL, JEM-2010). X-ray diffraction (XRD) patterns were conducted on a Bruker D2 Phaser X-ray diffractometer.

All electrochemical measurements were carried out with a CHI660E electrochemical workstation in a typical three-electrode setup, with a glass carbon electrode (GCE, 3 mm in diameter) coated with the catalyst ink as the working electrode, a graphite rod as the counter electrode, and an Ag/AgCl (sat. KCl) as the reference electrode. The catalyst ink was prepared by dispersing 5 mg of catalyst into 0.5 ml of solution containing 430 μL of water/ethanol (v/v = 4:1) and 70 μL of 5 wt% Nafion solution, followed by sonicated for at least 20 min to form a homogeneous ink solution. Then 5 μL of the catalyst ink was dropped onto the carbon cloth and dried at room temperature. (loading: <0.262 mg/cm^2). All the potentials were calibrated with respect to a reversible hydrogen electrode (RHE). In 0.5 mol/L H_2SO_4 (pH 0), E(RHE) = E(Ag/AgCl) + 0.232 V. In 1.0 mol/L KOH (pH 14), E(RHE) = E(Ag/AgCl) + 1.059 V. In 1.0 mol/L PBS (pH 7), E(RHE) = E(Ag/AgCl) + 0.646 V. Linear sweep voltammetry (LSV) measurements were conducted in electrolyte with a scan rate of 5 mV/s. Corresponding Tafel curves were calculated from the LSV data. Electrochemical impedance spectroscopy (EIS) measurements were performed at an overpotential of 160 mV with a frequency range from 0.01 Hz to 100 kHz. Cyclic voltammetry was used to estimate theelectrochemical double layer capacitance (Cdl) in nonfaradaic region from 0 to 0.1 V *vs*. RHE with different scan rates (20 – 140 mV/s). The Cdl was estimated by plotting $J = J_{anodic} - J_{cathodic}$ at 0.05 V *vs*. RHE against the scan rate. The linear slope is twice the Cdl. Electrochemical stability was measured using cyclic voltammetry (CV) sweeps at 50 mV/s between −0.4 V and −0.1 V *vs.* RHE for 2000 cycles. The current density – time (I–t) curves were carried out at overpotentials of 82, 102 and 261 mV in 0.5 mol/L H_2SO_4, 1.0 mol/L KOH and 1.0 mol/L PBS, respectively. All data were corrected using iR compensation.

Fig. 1 illustrates the synthesis process of the NiCoP hollow polyhedrons catalyst. ZIF-67 is prepared *via* a coprecipitation method under room temperature, and it exhibits distinct topological features with rhombic dodecahedron structure (Fig. 1b). In the first step, these ZIF-67 particles are dispersed in ethanol solution of $Ni(NO_3)_2$ and continuously stirred for 60 min to produce ZIF-67/Ni-Co LDH yolk-shelled structures (Fig. 1c). During the process, protons generated from the hydrolysis of Ni^{2+} ions can gradually etch ZIF-67 templates and the released Co^{2+} ions may be partially oxidized by dissolved O_2 and NO_3- ions in the solution. Then the Co^{2+}/Co^{3+} ions will coprecipitate with Ni^{2+} ions to form Ni-Co LDH shells [24]. Afterward, thermal calcination is applied during which the ZIF-67 cores and Ni-Co LDH shells can be converted into Co_3O_4 and $NiCo_2O_4$ yolk-shelled polyhedrons (Fig. 1d) [25], respectively. Because of the as-formed gap between ZIF-67 and Ni-Co LDH, possible strain between the cores and the shells generated during the calcination process that may result in

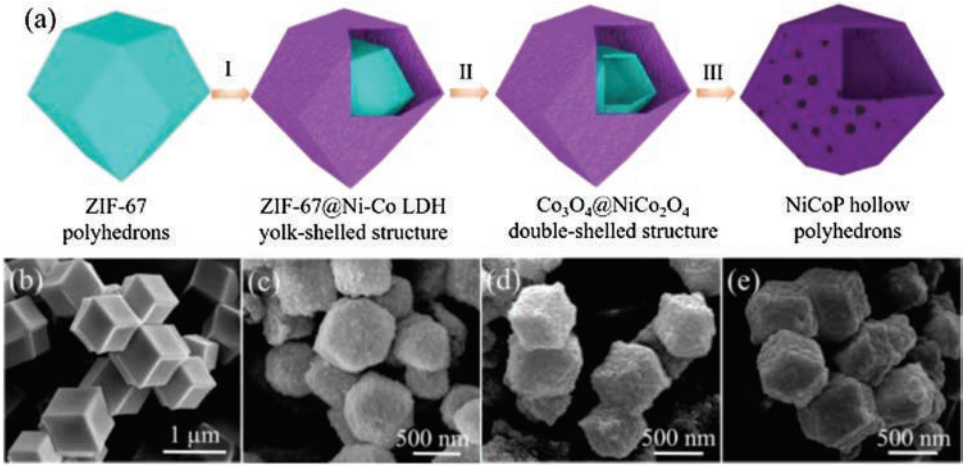

Fig. 1. (a) Schematic illustration of the synthesis process of NiCoP hollow polyhedrons. (b-e) SEM images of ZIF-67, ZIF-67/Ni-Co LDH, Co_3O_4@$NiCo_2O_4$ and NiCoP.

the collapse of the shells can be effectively alleviated. Finally, the phosphorization process is followed by which the as-prepared NiCoP hollow polyhedrons (Fig. 1e) are subsequently converted.

The XRD pattern of the ZIF-67 crystals matches well with previous reports, and the EDX result confirms the stoichiometry of the as-prepared crystals (Figs. S1a and b in Supporting information). FESEM and TEM images (Figs. S1c and d in Supporting information) reveal that the ZIF-67 particles show a polyhedral shape with a smooth surface and an average size of approximately 850 nm. According to the EDS elemental mapping (Fig. S1e in Supporting information) also revealed that Co, C, N elements were evenly distributed over the entire ZIF-67.

After reaction with $Ni(NO_3)_2$ in ethanol solution for 60 min, the particles still retain the polyhedral shape but exhibit the rougher surface constructed by small nanosheets (Figs. S2c and d in Supporting information) XRD pattern demonstrates these polyhedrons are still mainly ZIF-67 with diminished peak intensity, further confirmed by the EDX analysis (Figs. S2a and b in Supporting information). FESEM image of a particle with a broken outer shell (Fig. S2c) reveals that the inner core preserves the smooth surface. The distinctions between the shell and the core are further revealed by TEM observations (Fig. S2d) where the shell is composed of interconnected small nanosheets while the core appears similar to ZIF-67. According to the EDS elemental mapping (Fig. S2e in Supporting information) also revealed that Co, Ni, C, N elements were evenly distributed over the entire ZIF-67.

XRD pattern of the annealed product of ZIF-67/Ni-Co LDH yolk-shelled structures confirms the formation of the spinel type oxides containing Ni and Co (Figs. S3a and b in Supporting information). From the panoramic FESEM image (Fig. S3c in Supporting information), the annealed product inherits the polyhedral shape from the ZIF-67/Ni-Co LDH yolk-shelled structures. Furthermore, the inner shell can be well identified from some particles with broken outer shells (Fig. S3c). From TEM observations (Fig. S3d in Supporting information), the yolk-shelled polyhedrons derived from the Ni-Co LDH do not shrink significantly whereas the inner polyhedrons derived from ZIF-67 show significant shrinkage with decreased size compared with the original ZIF-67 cores. The thickness of the shells has been determined by TEM observation under higher magnification. As shown in Fig. S3d, the thickness of the outer $NiCo_2O_4$ shell is about 250 nm while the inner Co_3O_4 shell shows similar thickness but with a very uneven surface. The spatial distribution of different elements in the $Co_3O_4/NiCo_2O_4$ yolk-shelled polyhedrons is investigated by elemental mapping analysis on representative $Co_3O_4/NiCo_2O_4$ yolk-shelled polyhedrons under TEM observation. The elemental mapping results indicate that Co and O (Fig. S3e in Supporting information) are distributed homogeneously in both the outer shell and the inner shell with some apparent enhancement in the central region. On the contrary, the signal intensity of Ni (Fig. S3e) is very uniform throughout the region without any enhancement in the central area where the inner Co_3O_4 polyhedrons locates, indicating the inner shell is free of Ni. Thus, these EDX results further verify that the inner shell mainly consists of Co_3O_4, and the outer shell is composed of $NiCo_2O_4$, confirming the successful formation of materials with different shell compositions.

After the phosphidation of $Co_3O_4/NiCo_2O_4$ yolk-shelled polyhedrons, SEM image in Fig. 2a shows that the morphology of polyhedrons is well maintained, and the hollow structure can be clearly observed in Fig. 2b. The original core-shell structure was transformed into hollow structure. It can be further observed in the transmission electron microscope image corresponding to Fig. 2b that the inner core Co_3O_4 polyhedrons structure has been highly granular before being phosphatized, so the inner core has become agglomerated after higher-temperature phosphating process. The HRTEM image shows distinct lattice fringes with an interplanar spacing of 0.205 nm, corresponding well to the (321) lattice plane of the CoP3, whereas the lattice spacing of 0.195 nm and 0.173 nm can be ascribed to the (210) and (300) plane of the Ni_2P phase (Fig. 2c), confirming the formation of the heterostructure [26]. The EDX elemental mapping images (Fig. 2d) confirm the even distributions of Ni, Co, and P elements throughout the whole shell of the polyhedrons. The Co_3O_4 polyhedrons were obtained by calcining ZIF67 in air (Fig. S4 in Supporting information). And then CoP polyhedrons were obtained by phosphating Co_3O_4 (Fig. S5 in Supporting information). The ZIF-67/Ni-Co LDH yolk-shelled

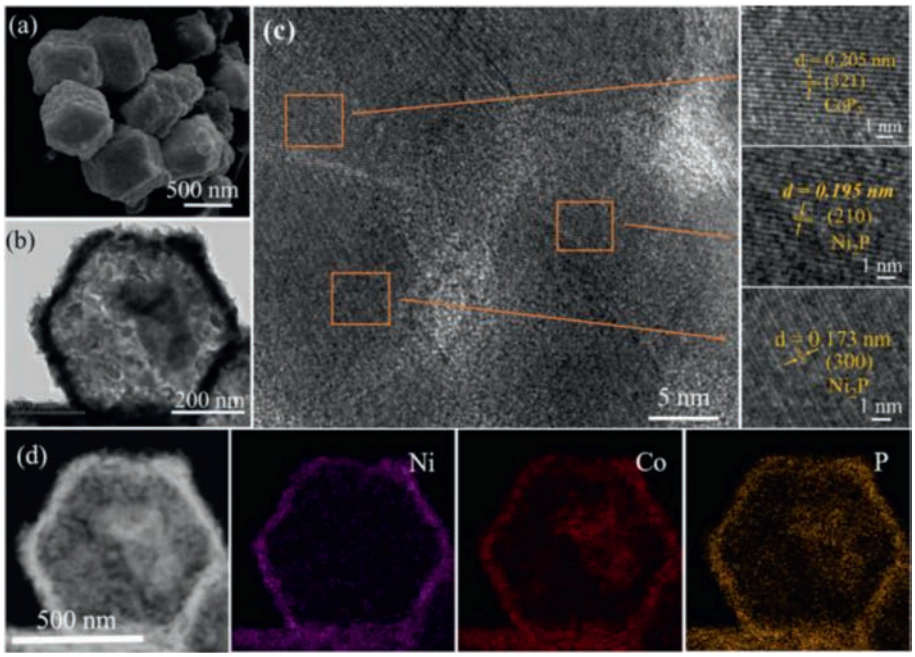

Fig. 2. (a) SEM image of NiCoP hollow polyhedrons. (b) TEM image of NiCoP hollow polyhedrons. (c) HRTEM images of NiCoP hollow polyhedrons. (d) EDX elemental mapping images of NiCoP hollow polyhedrons.

structures will reunite without being calcined in air, so the crystal structure of the material after calcination will become more stable (Fig. S6 in Supporting information).

XRD in Fig. 3a presents the diffraction peaks at around 40.8°, 44.6°, 47.3°, 54.9°, 74.6°, 80.9° which can be well-indexed to CoP_3 (JCPDS No. 27-1121), the diffraction peaks at around 40.5°, 43.9°, 47.1°, 50.2°, 53.1°, 61.3°, 80.9° which can be well-indexed to Ni_2P (JCPDS No. 03-0953), demonstrating that NiCoP hollow polyhedrons is composed of CoP_3 and Ni_2P [27–29]. The XPS survey spectrum of NiCoP hollow polyhedrons in Fig. S3 indicates the presence of Ni, Co, P, C and N. The chemical state and surface compositions of the NiCoP hollow polyhedrons are analyzed by XPS. For the Co $2p_{3/2}$ (Fig. 3b), the binding energies at 776.6, 782.5 and 787.1 eV are attributed to Co-P, oxidized Co species, and satellite peak, respectively. Similarly, the binding energies at 797.5, 799.2 and 803.6 eV for the Co $2p_{1/2}$ can be ascribed to Co-P, oxidized Co species and satellite peak, respectively. For the Ni $2p_{3/2}$ (Fig. 3c), the binding energies at 853.6, 857.2, and 862.3 eV are attributed to Ni-P, oxidized Ni species, and satellite peak, respectively. Besides, the binding energies at 871.2, 875.1, and 881.3 eV for the Ni $2p_{1/2}$ can be ascribed to Ni-P, oxidized Ni species, and satellite peak, respectively. For the P 2p (Fig. 3d), the doublet at 128.8 and 130.1 eV can be attributed to Ni-P or Co-P in metal phosphide [30,31]. These results indicate that Co and Ni have positive charges (δ^+), while the P has a negative charge (δ^-), suggesting the existence of electron density transfer from Co and Ni to P.

The HER performances of all the samples were firstly tested in a 0.5 mol/L H_2SO_4 solution. The linear sweep voltammetric (LSV) curves shown in Fig. 4a suggest that NiCoP hollow polyhedrons is superior to Co_3O_4, Co_3O_4@$NiCo_2O_4$, and CoP in all the range of testing potentials. Co_3O_4 exhibits the lowest performance with a current density of 10 mA/cm^2 even at an overpotential of about 421 mV. NiCoP hollow polyhedrons only needs an overpotential of 82 mV to achieve 10 mA/cm^2, far lower than those of Co_3O_4@$NiCo_2O_4$ (282 mV) and CoP (185 mV), close to that of commercial Pt/C catalyst (56 mV). The HER kinetics of the above catalysts are verified by the corresponding Tafel slopes, and a lower Tafel slope will lead to a faster increment of HER rate with increasing overpotential. As shown in Fig. 4b, the NiCoP hollow polyhedrons delivers a Tafel slope of < 72 mV/dec, suggesting that the corresponding HER abides by a Volmer–Heyrovsky mechanism [32,33], and the electrochemical desorption process could be the rate-limiting step. It can be found that the Tafel slope of NiCoP hollow polyhedrons is larger than that of Pt/C (49 mV/dec) but obviously smaller than those of CoP (89 mV/dec), Co_3O_4@$NiCo_2O_4$ (248 mV/dec) and Co_3O_4 (301 mV/dec). As the Tafel slope is directly associated with the reaction kinetics of electrocatalysts, the lower Tafel slope for NiCoP hollow polyhedrons implies its faster catalytic kinetics and higher catalytic activity toward HER as compared with other samples. The electrical impedance spectroscopy (EIS) was carried out to study the catalysts' conductivity as well as the mass transport between the electrode and electrolyte. The Nyquist plots shown in Fig. 4c show that the charge transfer resistance (R_{ct}, the semicircles in the higher frequency range) of NiCoP/C hollowpolyhedrons is far smaller than those of CoP, Co_3O_4 and Co_3O_4@$NiCo_2O_4$. The order of the mass transfer resistance (R_{mt}, the semicircles in the lowest frequency range) is NiCoP < CoP < Co_3O_4@$NiCo_2O_4$. In addition, the double-layer capacitance (C_{dl}) was probed to estimate the electrochemically active surface areas (ECSA) and the corresponding intrinsic activity. The CV curves of NiCoP, CoP, Co_3O_4 and Co_3O_4@$NiCo_2O_4$ with different scan rates in a non-faradaic region from 0 to 0.1 V *vs.* RHE are shown in Fig. S8 (Supporting information). As presented in Fig. 4d, NiCoP hollow polyhedrons exhibits a slope of 23.8 mF/cm^2, much larger than those of CoP (14.9 mF/cm^2), Co3O4 (2.97 mF/cm^2) and Co_3O_4@$NiCo_2O_4$. These prove that NiCoP hollow polyhedrons expose more effective active sites at the solid – liquid interface, resulting in higher electrochemical HER activity. Continuous CV with a potential range from −0.4 V to −0.1 V (*vs.* RHE) scanning was conducted with the scan rate of 50 mV/s, and the negligible difference could be observed after 2000 cycles (Fig. 4e). The excellent long-term stability of the NiCoP hollow polyhedrons

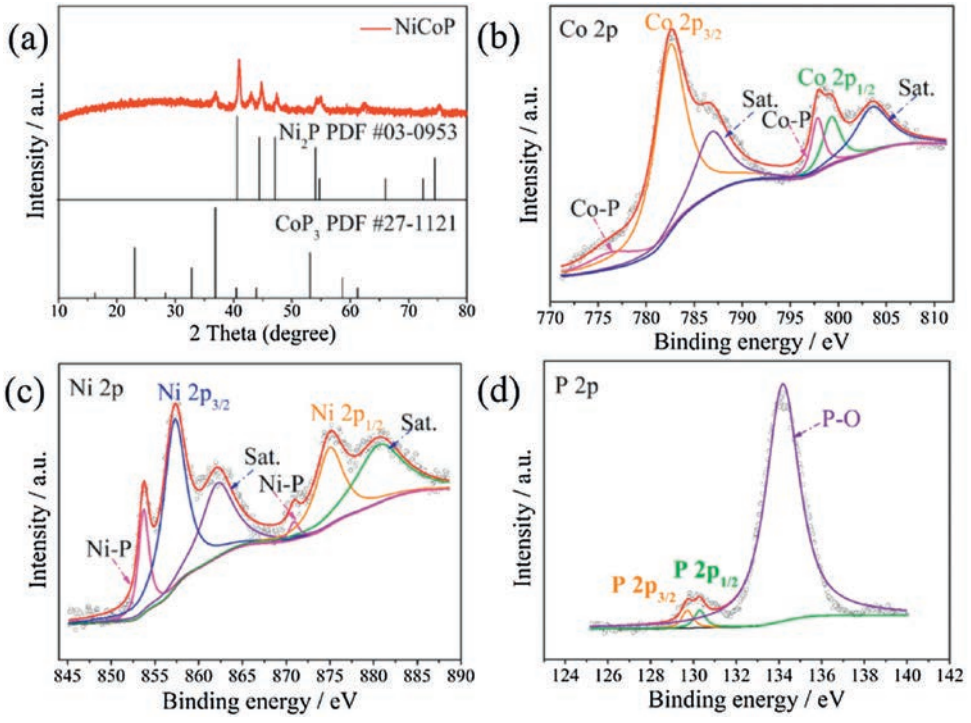

Fig. 3. (a) XRD pattern of the as-prepared sample. High-resolution XPS spectra of (b) Co 2p, (c) Ni 2p and (d) P 2p region for the NiCoP hollow polyhedrons.

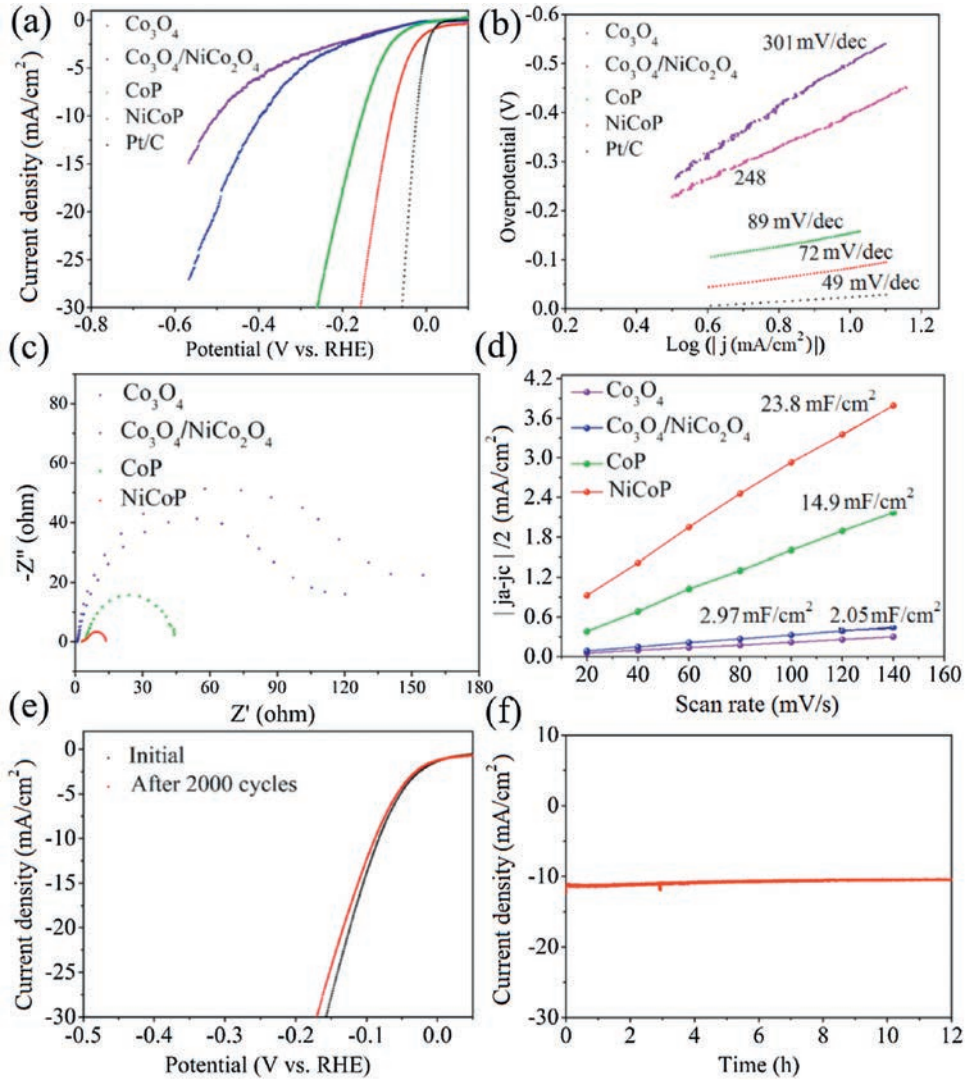

Fig. 4. (a) LSV curves of Co_3O_4, $Co_3O_4/NiCo_2O_4$, CoP, NiCoP and Pt/C. (b) Tafel slopes of Co_3O_4, $Co_3O_4/NiCo_2O_4$, CoP, NiCoP and Pt/C. (c) Nyquist plots of Co_3O_4, $Co_3O_4/NiCo_2O_4$, CoP and NiCoP. (d) Current density differences plotted against scan rates of Co_3O_4, $Co_3O_4/NiCo_2O_4$, CoP and NiCoP. (e) Continuous CV curves and (f) chronopotentiometry of NiCoP in 0.5 mol/L H_2SO_4.

catalyst is further confirmed by chronoamperometric investigation at an overpotential of 150 mV in 0.5 mol/L H_2SO_4. From the polarization curves in Fig. 4f, the current density at 12 h is < 92% of the initial value. The excellent stability is probably associated with the good compositional and structural stability of NiCoP hollow polyhedrons [34–37].

The performances of CoP/Co-MOF toward HER were also studied in 1 mol/L KOH and 1 mol/L PBS solution, separately. Fig. S9a (Supporting information) shows the LSV curves of each catalyst in 1 mol/L KOH. The performance of Co_3O_4 is too poor to be detected in -0.6 V to 0 V. NiCoP hollow polyhedrons exhibits an overpotential of 102 mV to achieve the current density of 10 mA/cm^2, close to that of Pt/C (69 mV), much smaller than those of Co_3O_4@$NiCo_2O_4$ (314 mV) and CoP (194 mV). Fig. S9b (Supporting information) indicates that NiCoP hollow polyhedrons possesses the fastest dynamics with the Tafel slope of 101 mV/dec, close to Pt/C of 59 mV/dec, lower than those of CoP (132 mV/dec) and Co_3O_4@$NiCo_2O_4$ (196 mV/dec). Remarkably, the NiCoP hollow polyhedrons still exhibits good stability and durability even in such acid medium. After 2000 continuous CV cycles in 1 mol/L KOH, the polarization curves of NiCoP hollow polyhedrons show little loss, and the overpotential slightly increases at 10 mA/cm^2 (Fig. S9c in Supporting information). Furthermore, the time-dependent current density curve at a static overpotential of 150 mV *vs.* RHE indicates that NiCoP hollow polyhedrons can retain its catalytic activity for at least 12 h (Fig. S9d in Supporting information). The HER performance of the NiCoP hollow polyhedrons in 1.0 mol/L PBS are investigated as showed in Fig. S9e (Supporting information). The NiCoP hollow polyhedrons demands a relatively high overpotential of 261 mV to achieve a current density of 10 mA/cm^2, whereas other samples have overpotentials of > 400 mV at the same current density. It is worth noting that all the samples show different polarization curves in neutral electrolyte compared to those in alkaline or acidic electrolyte. This might be associated with a higher solution resistance and less effective proton transport in neutral medium, and the exact reason is not completely understood at present time. Fig. S9f (Supporting information) indicates that NiCoP hollow polyhedrons possesses the fastest dynamics with the Tafel slope of 176 mV/dec, lower than those of CoP (218 mV/dec) and Co_3O_4@$NiCo_2O_4$ (325 mV/dec). All the above results demonstrate that the NiCoP hollow polyhedrons electrocatalyst can be used as a pH universal electrocatalyst with

high HER activity and good stability, and its property is comparable and even superior to those of other non-noble metal HER electrocatalysts that can be applied under alkaline, acidic, or neutral conditions. The all-pH applicability of the NiCoP hollow polyhedrons electrocatalyst permits it to be utilized in different water electrolysis technologies [38–43], such as water – alkali and chlor – alkali electrolyzers [44–47], the proton exchange membrane cells (acidic conditions) [48–52], and microbial electrolysis cells (neutral conditions) [53–58].

In summary, NiCoP hollow and porous polyhedrons have been synthesized by acidic etching and precipitation of ZIF-67 polyhedron and further phosphorization treatment with NaH_2PO_2. Benefiting from the synergistic effects of metal ions and the well-defined porous polyhedron structure, the as-synthesized NiCoP hollow polyhedrons shows better electrochemical properties and mechanical stability for hydrogen evolution reaction over a pH-universal range, with a small Tafel slopes of 72, 101, 176 mV/dec, and a low overpotential of 82, 102, 261 mV at a current density of 10 mA/cm^2 in 0.5 mol/L H_2SO_4, 1 mol/L KOH and 1 mol/L PBS. This work demonstrates a promising route to achieve high-performance and low-cost CoP-based electrocatalysts for hydrogen evolution in wide pH conditions.

Declaration of competing interest

The authors report no declarations of interest.

Acknowledgments

This work was supported by the National Natural Science Foundation of China (Nos. 51672109, 51802177), the Independent Cultivation Program of Innovation Team of Ji'nan City (No. 2019GXRC011), and Natural Science Foundation of Shandong Province (No. ZR2018BEM019). All the authors discussed the results and commented on the manuscript.

Appendix A. Supplementary data

Supplementary material related to this article can be found, in the online version, at doi:https://doi.org/10.1016/j.cclet.2020.10.046.

References

[1] Y. Xie, M. Chen, M. Cai, et al., Inorg. Chem. 58 (2019) 14652–14659.
[2] D.V. Shinde, L.D. Trizio, Z. Dang, et al., Chem. Mater. 29 (2017) 7032–7041.
[3] J. Duan, Y. Zou, Z. Li, et al., J. Electroanal. Chem. 847 (2019) 113187.
[4] A.M. El-Toni, M.A. Habila, J.P. Labis, et al., Nanoscale 8 (2016) 2510–2531.
[5] X. Wang, L. Yu, B.Y. Guan, et al., Adv. Mater. 30 (2018) 1801211.
[6] Y. Lu, Y. Deng, S. Lu, et al., Nanoscale 11 (2019) 21259–21265.
[7] J. Hu, J. Chen, H. Lin, et al., J. Solid State Chem. 259 (2018) 1–4.
[8] J. Hao, W. Yang, Z. Zhang, et al., Nanoscale 7 (2015) 11055–11062.
[9] B.Y. Guan, X.Y. Yu, H.B. Wu, et al., Adv. Mater. 29 (2017) 1703614.
[10] Y. Feng, X.Y. Yu, U. Paik, Chem. Commun. 52 (2016) 6269–6272.
[11] J. Jiang, L. Zhu, Y. Sun, et al., J. Power Sources 426 (2019) 74–83.
[12] X. Gao, H. Zhang, Q. Li, et al., Angew. Chem. Int. Ed. 55 (2016) 6290–6294.
[13] K. An, S.G. Kwon, M. Park, et al., Nano Lett. 8 (2008) 4252–4258.
[14] R. Wu, X. Qian, X. Rui, et al., Small 10 (2014) 1932–1938.
[15] J. Li, S. Lu, H. Huang, et al., ACS Sustain. Chem. Eng. 6 (2018) 10021–10029.
[16] L. Li, W. Xie, J. Chen, et al., J. Solid State Chem. 264 (2018) 1–5.
[17] S. Payra, S. Challagulla, C. Chakraborty, et al., J. Electroanal. Chem. 853 (2019) 113545.
[18] L. Han, T. Yu, W. Lei, et al., J. Mater. Chem. A 5 (2017) 16568–16572.
[19] Z. Li, M. Shao, L. Zhou, et al., Nano Energy 25 (2016) 100–109.
[20] M. Guo, Y. Qu, F. Zeng, et al., Electrochim. Acta 292 (2018) 88–97.
[21] P. Jiang, Q. Liu, C. Ge, et al., J. Mater. Chem. A 2 (2014) 14634–14640.
[22] Y. Feng, X.Y. Yu, U. Paik, Chem. Commun. 52 (2016) 1633–1636.
[23] J. Qin, S. Wang, X. Wang, Appl. Catal. B: Environ. 209 (2017) 476–482.
[24] X. Cai, X. Shen, L. Ma, et al., Chem. Eng. J. 268 (2015) 251–259.
[25] H. Hu, B. Guan, B.Y. Xia, et al., J. Am. Chem. Soc. 137 (2015) 5590–5595.
[26] G. Zhao, K. Rui, S.X. Dou, et al., Adv. Funct. Mater. 28 (2018) 1803291.
[27] T. Wu, M. Pi, X. Wang, et al., J. Alloys Compd. 729 (2017) 203–209.
[28] H. Sun, X. Xu, Z. Yan, et al., Chem. Mater. 29 (2017) 8539–8547.
[29] Y. Shi, Y. Xu, S. Zhuo, et al., ACS Appl. Mater. Interfaces 7 (2015) 2376–2384.
[30] Y. Lin, K. Sun, S. Liu, et al., Adv. Energy Mater. 9 (2019) 1901213.
[31] H. Liu, X. Ma, H. Hu, et al., ACS Appl. Mater. Interfaces 11 (2019) 15528–15536.
[32] H. Du, R.M. Kong, X. Guo, et al., Nanoscale 10 (2018) 21617–21624.
[33] L. Feng, H. Vrubel, M. Bensimon, X. Hu, Phys. Chem. Chem. Phys. 16 (2014) 5917–5921.
[34] M.B. Gawande, A. Goswami, T. Asefa, et al., Chem. Soc. Rev. 44 (2015) 7540–7590.
[35] W. Li, S. Zhang, Q. Fan, et al., Nanoscale 9 (2017) 5677–5685.
[36] J. Wang, W. Cui, Q. Liu, et al., Adv. Mater. 28 (2016) 215–230.
[37] P. Xiao, W. Chen, X. Wang, Adv. Energy Mater. 5 (2015) 1500985.
[38] Y. Li, J. Liu, C. Chen, X. Zhang, J. Chen, ACS Appl. Mater. Interfaces 9 (2017) 5982–5991.
[39] Y. Yin, R.M. Rioux, C.K. Erdonmez, et al., Science 304 (2004) 711–714.
[40] X.Y. Yu, Y. Feng, Y. Jeon, et al., Adv. Mater. 28 (2016) 9006–9011.
[41] J. Zhang, L. Zhang, X. Wang, W. Zhu, Z. Zhuang, Chem. Commun. 56 (2020) 90–93.
[42] Y.X. Zhu, L. Zhang, G.G. Zhu, X. Zhang, S.Y. Lu, Nanoscale 12 (2020) 5848–5856.
[43] Y. Meng, P. Sun, W. He, B. Teng, X. Xu, Nanoscale 11 (2019) 688–697.
[44] W. He, G. Zhao, P. Sun, et al., Nano Energy 56 (2019) 207–215.
[45] R. Cao, H. Yang, S. Zhang, X. Xu, Appl. Catal. B: Environ. 258 (2019) 117997.
[46] G.L. Lu, X.B. Huang, Y. Li, et al., J. Energy Chem. 43 (2020) 8–15.
[47] G. Zhao, S.H. Hao, J.H. Guo, et al., Chin. J. Catal. 42 (2021) 501–509.
[48] H.Y. Zheng, X.B. Huang, Z.Y. Wu, et al., Chem. Asian J. 12 (2017) 2956–2961.
[49] Y.Q. Jia, J.Q. Xie, Y. Yang, et al., Chin. Chem. Lett. 31 (2020) 855–858.
[50] H.Y. Zheng, X.B. Huang, H.Y. Gao, et al., Chem. Eur. J. 25 (2019) 1083–1089.
[51] G. Zhao, Y.M. Chen, P.X. Sun, et al., Nanoscale 12 (2020) 17849–17857.
[52] H.Y. Zheng, X.B. Huang, H.Y. Gao, et al., Appl. Surface Sci. 479 (2019) 1254–1261.
[53] L. Jiang, Z.Y. Wu, Y.N. Wang, et al., ACS Nano 13 (2019) 10376–10385.
[54] P.Y. Yang, Z.Y. Wu, Y.C. Jiang, et al., Adv. Energy Mater. 8 (2018) 1801392.
[55] Y.C. Jiang, Z.Y. Wu, L. Jiang, et al., Nanoscale 10 (2018) 12003–12010.
[56] Y.C. Jiang, Y. Song, Y.M. Li, et al., ACS Appl. Mater. Interfaces 9 (2017) 37645–37654.
[57] M. Li, L. Xiao, D. Wang, et al., Chin. Chem. Lett. 30 (2019) 2328–2332.
[58] Y.Q. Jiang, J.P. Liu, Energy Environ. Mater. 2 (2019) 30–37.